Development of a tunable polarimetric scatterometry system in the MWIR and LWIR

Thomas M. Fitzgerald, Michael A. Marciniak and Stephen E. Nauyoks

Department of Engineering Physics
Air Force Institute of Technology
Wright-Patterson AFB OH 45433-7765

ABSTRACT

A unique **tunable polarimetric scatterometry** system has been developed by upgrading a Schmitt Measurement Systems Complete Angle Scatter Instrument (CASI) to produce a **Dual-Rotating-Retarder full-Mueller-matrix polarimeter**. The system has been enhanced by automation, addition of multiple, tunable, laser light sources, an improved sample positioning and orientation interface, and enhanced data-analysis software. A primary application of this system is the characterization of novel nano- and micro-structured materials, such as **photonic crystals, plasmonic structures** and **optical meta-materials**, which often display very narrow-band performance. The ability to characterize these materials both at and away-from their resonances is a clear advantage. The specific project goals are to demonstrate (1) a novel nano- and micro-structured-material-characterization full-polarimetric-**diffuse-ellipsometry** technique suitable to measure desired material properties with stated uncertainty limits for novel optical material structures of interest, and (2) the incorporation of predictive computational codes that estimate the electro-magnetic property values for novel nano- and micro-structured-material designs and concepts of interest.

Keywords: Polarimetric scatterometry, MWIR, LWIR, metamaterial, plasmonics, photonic crystals, Dual-Rotating-Retarder polarimeter, diffuse ellipsometry

1. INTRODUCTION

1.1 Background

Nano-scale-structured materials with sub-wavelength features can have enhanced or novel spectrally dependent values for infrared permeability and permittivity. Optimized nano-scale features cause wavelength dependent absorption, scatter, and overall extinction features not present in the bulk material. Such structures are often referred to as metamaterials, but may also include other plasmonic structures or photonic crystals. The application space of engineered metamaterials includes sub-wavelength waveguides and antennas, true time delay devices, optical and infrared filters, and plasmonic-enabled electronic-optical interfaces.[1]

1.2 Motivation

This paper presents the development of a novel infrared (IR) metamaterial characterization technique for measuring and analyzing full-angle full-polarimetric scatter (i.e. both transmittance and reflectance distribution) from metamaterials of interest. The technique expands the domain of Mueller-matrix ellipsometry. Current commercial Mueller-matrix ellipsometers, such as IR-VASE by Woollam, only operate at the specular reflection angle. The approach presented here is an evolutionary continuation of the in-specular-plane-but-not-at-the-specular-angle and out-of-specular-plane work by Germer *et al*. at NIST and others.[2-5] The research presented here extends the current state-of-the-art characterization technique to novel IR metamaterials. Appropriate numerical scatter models are incorporated for the as-built mid-wave IR (MWIR, ~3-6.5 μm) or long-wave IR (LWIR, ~7.4-12 μm) metamaterial architecture, to include the effects of nano-scale geometry and fabrication defects. The goal is to bridge the gap between metamaterial design performance and metamaterial "as-built" performance.

Multiple Daylight Solutions® quantum cascade laser (QCL) sources have been added to the Schmitt Measurement Systems Complete Angle Scatter Instrument (CASI) Dual-Rotating-Retarder (DRR) full-polarimetric scatter system in order to facilitate spectral probing of metamaterials through the MWIR and LWIR spectral regions. The previously presented system enhancements for automation, improved sample positioning, and data analysis are extended to the spectral domain.[4, 5] The advantage of discrete laser sources for full-spectral coverage is much larger signal-to-noise ratios at all desired wavelengths of operation as compared to a broadband infrared source.

Measured material property values for permittivity and permeability are used to derive macro property values such as impedance and index of refraction. The full scatter angle Mueller-matrix measurements made possible by this instrument capture the complete interaction of a metamaterial with incident energy. The measured Mueller-matrix stores the degree of attenuation, de-polarization and retardance for all angles of interest, both incident and scatter. The currently accepted technique for measuring metamaterial permittivity and permeability uses normal-incidence polarized light to determine the reflection and transmission coefficients of the metamaterial. Then, the permittivity and permeability are estimated.[6]

Mueller-matrix ellipsometry requires strong predictive models in order to properly interpret the results. The DDSCAT Direct Dipole Approximation (DDA) based computational model is incorporated to develop scatter predictions for the metamaterial geometry of interest. This model provides an understanding of the CASI-DRR-measured scatter due to imperfect fabrication and layer defects, as well as possible diffraction due to device structure. The finite-element model provides absorption and scattering coefficients for the desired geometry based on a selected input field, $E(\mathbf{k},\lambda)$, where $\mathbf{k}$ gives the incident propagation vector and λ is the optical wavelength in air.

This approach to metamaterials property prediction, structure fabrication and optical measurement is broadly applicable to diagnostics or polarimetric mode excitation of optical metamaterial structures, as well as other nano-structured materials, from the visible through the LWIR.

2. METHODOLOGY

2.1 Description of the modified CASI-DRR instrument

The CASI bi-directional scatter distribution function (BSDF) measurement system was modified to the DRR configuration proposed by Azzam[7] and further developed by Goldstein and Chipman,[8] and Smith.[9] Here, "bidirectional" means light from any incident direction is measured as it is scattered into all directions for both the transmission and reflection hemispheres, and the BSDF is the combination of the bidirectional transmittance distribution function (BTDF) and the bidirectional reflectance distribution function (BRDF). The DRR addition consists of an input polarization state generator and an output polarization state analyzer. The generator and analyzer stages each feature a linear polarizer and a linear retarder. The linear retarders are rotated to generate and analyze complete polarization states. The analyzer stage features rotational motion in a horizontal plane about the sample (*i.e.* in the plane of incidence). The representative optical layout for the instrument is shown in Figure 1 where sample, M, has the necessary six degrees of freedom required for full scatter characterization and detailed and named in Figure 2. The DRR application summarized to our particular adaptation is presented in the Theory section that follows.

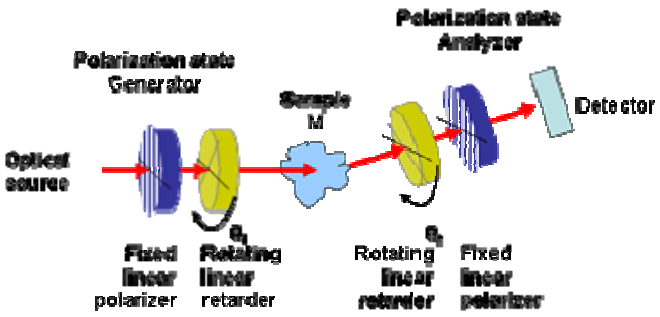

Figure 1. Optical configuration for AFIT DRR

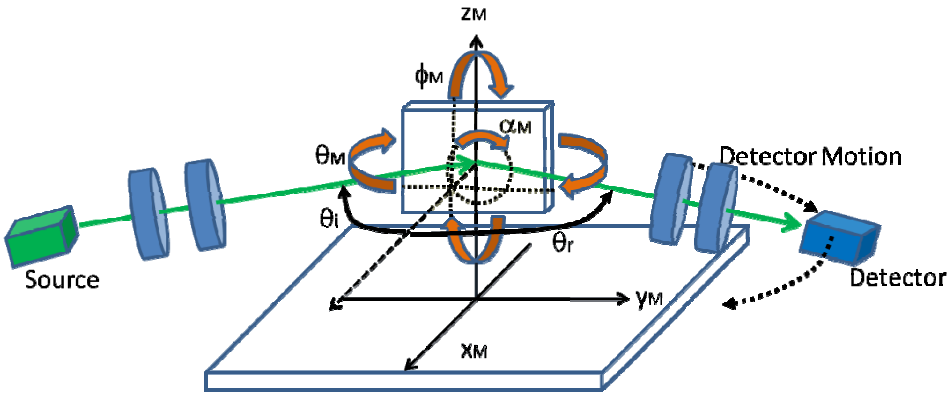

Figure 2. Geometry naming convention for AFIT DRR degrees of freedom

2.2 Mechanical improvements

Four high-precision Aerotech AGR-50 rotary stages were added and electronically integrated to the CASI instrument to achieve DRR configuration (Fig. 3). These stages automate the rotational motion of two spectrally matched linear polarizers and (nominally) quarter-wave plates (*i.e.* retarders). The AGR-50 has an internal 50:1 angular reduction ratio giving a calculated repeatable step size of 0.016° when driven by a 0.8° increment stepper motors. This is well within the 0.3° accuracy recommended by Goldstein.[8]

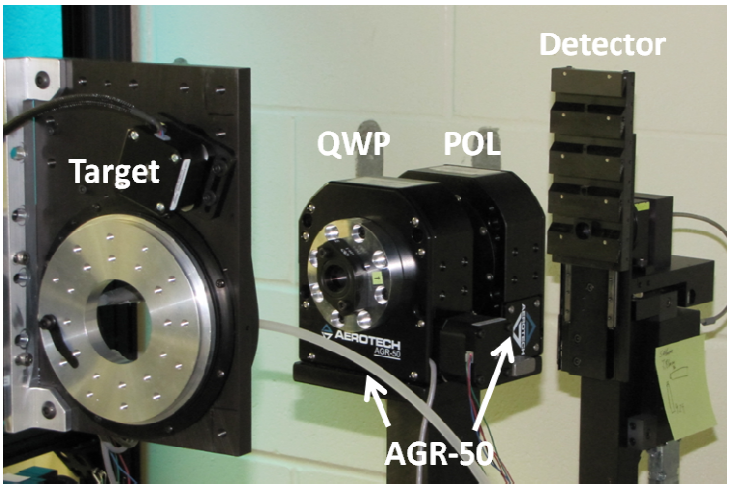

Figure 3. Two Aerotech AGR-50 mounted in Analyzer stage of AFIT DRR. Two additional AGR-50s are mounted in the Generator stage.

2.3 Description of the spectral source improvements

Six Daylight Solutions external cavity Bragg-tunable QCL's that cumulatively cover the wavelength ranges of 4.4-6.5 and 7.4-9.7 μm are being integrated as spectral sources to the modified DRR system. The QCL's are water cooled and non-cryogenic. They offer a small individual footprint for each unit. An example unit is shown in Figure 4. Each laser head is connected by an umbilical cord to the laser controller that selects wavelength output. Laser wavelength is able to be set to six significant digits with w relative uncertainty of less than 0.2%. Laser line-widths are less than 30 MHz CW and 30 GHz pulsed. The particular spectral output and power levels for each source is shown in Figure 5.

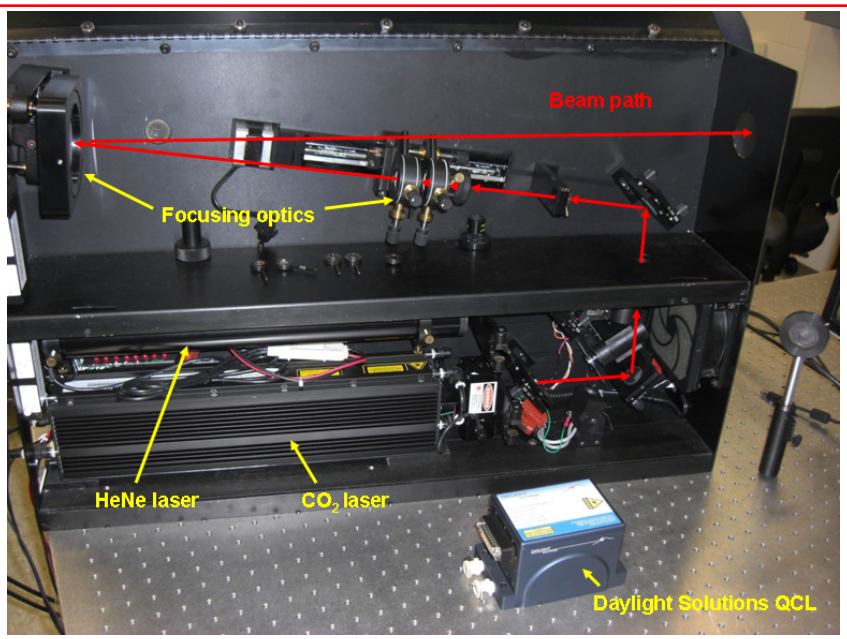

Figure 4. QCL source from Daylight Solutions shown beside AFIT DRR laser source box.

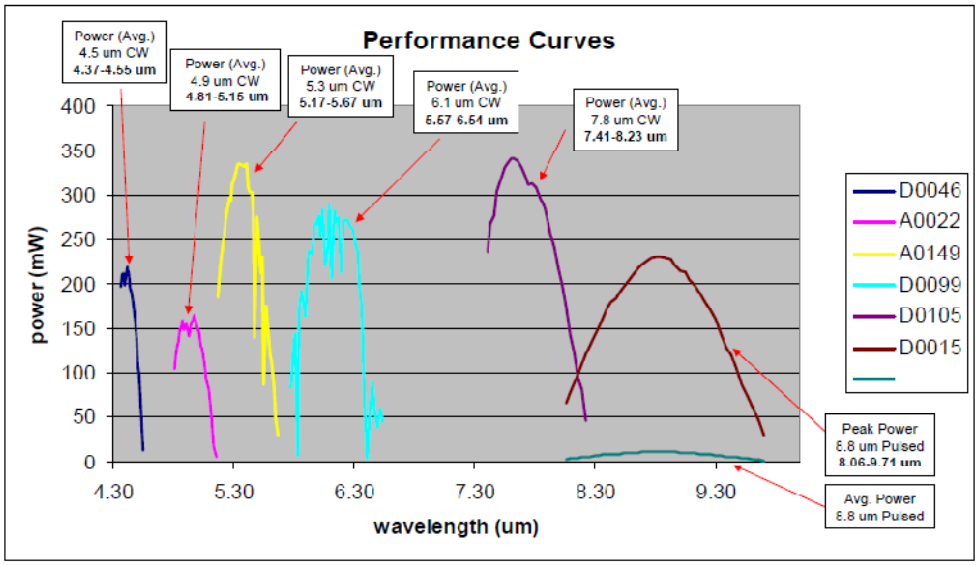

Figure 5. Spectral range coverage and average power emission for each of the six Daylight Solutions QCL sources.[10]

2.4 Description of the data analysis implementation

The measurement planning, measurement analysis, and data presentation tools are coded in Python 2.6. Python is an open-source object oriented scripting language that is scientifically extensible through external open-source add-ins like Scipy, Numpy WXpython, and Matplotlib. The Numpy and Scipy packages provide robust matrix algebra capability for complex numbers and methods, numeric matrix inversion, and parameter optimization through cost function minimization. Matplotlib is a native Python professional quality plotting and graphing package with MATLAB™-like syntax. WXPython provides a graphical user interface to facilitate use of the data planning, collection, and data analysis.

3. THEORY

3.1 Condition number theory

The condition number DRR instrument analysis approach by Smith was applied to define the AFIT DRR instrument operating mode.[9] In the Mueller algebra, the off-specular-plane DRR instrument measurement can be described by

$$I = (1000)\Pi_a \Delta_a(\theta_a, \delta_a) M(\theta_M, \phi_M, \alpha_M, x, y, z, \Omega_s) \Delta_g(\theta_g, \delta_g) \Pi_g S^T \qquad (1)$$

where I is the measured intensity or Stokes S_0 parameter of the output polarization state (mathematically selected by (1 0 0 0)), Π is the Mueller matrix for a polarizer, Δ is the Mueller matrix for a wave-plate at angle, θ, to the polarization axis with δ phase retardation, subscripts, a and g, refer to analyzer and generator elements, respectively, M is the Mueller matrix for the sample of interest with orientation (θ_M, ϕ_M, α_M, x, y, z) in the target reference frame. θ_M is the relative angle of rotation of the sample in the beam plane. ϕ_M is the out-of-plane rotation angle of the sample. (α_M, x, y, z) are the target orientation angle and absolute position necessary to define the orientation and location of a particular sample to be measured. Ω_s is the solid angle of scattered radiation. S is the Stokes vector of the input light. Equation 1 can be recast into the so-called W-Matrix form[11]

$$I = W(\theta_a, \delta_a, \delta_g, \theta_g) M \qquad (2)$$

where W is an [N x16] matrix that fully describes the instrument configuration for any desired generator-retarder/analyzer retarder combination. N is the number of independent measurements (typically 16 or more) necessary to return a full Mueller matrix. The W-matrix may then be inverted to deliver the Mueller matrix of the sample, M:

$$M = \left(W^T W\right)^{-1} W^T I \qquad (2)$$

Smith's condition number approach to W-Matrix analysis allows determination of both N and suitable angle-increment pairs for rotation of the linear retarders. From an analysis of the entire space of possible angle pairs, Smith showed that 34° and 26° increments for the generator and analyzer retarders, respectively, are optimal for pseudo-inversion of the W-matrix.[9] At present, we are using this angular combination in the AFIT DRR.

A W-Matrix analysis does not include effects of instrument scatter or optical component misalignment. These are areas of active research and discussion for our team. Applying the Compain DRR instrument characterization and error correction technique helps correct for systematic alignment errors in the instrument.[12] Finally, the spectrometric Mueller measurement technique described by Chenault has been applied to determine diattenuation and retardance values for all of the polarization components.[13]

3.2 The DDSCAT and Lumerical models

The modeling methods used for this research are Discrete Dipole Approximation (DDA) and Finite Difference Time Domain (FDTD). The DDA was developed by Purcell and implemented by Draine as DDSCAT.[14,15] DDSCAT uses a hybrid finite-element/coupled dipole method (FE/CDM) approach. The DDA finite elements are point polarized dipoles on a cubic lattice. The geometry and material-dependent spectral scatter and absorption coefficients are calculated.[16] DDSCAT has successfully determined localized nano-scale modes that support surface plasmon resonance for nano-particle bio- and chem-sensor development and interstellar spectroscopy of microscopic graphite. This capability makes it appealing for the spectrometric research proposed here. DDSCAT also has a proven record in optical metamaterial design and analysis. [17-29] Published DDSCAT results demonstrate much higher localized field strengths due to near-field

interactions, non-bulk material effects such as geometrically dependent local surface plasmon resonances, and interaction between the incident field and the structure geometry.[30-33] Fig. 6 shows the increased E-field calculated for interaction between a field at 0.544 μm and a 50-nm particle of either silver or a dielectric. DDSCAT can also be used to determine the extinction (scattering and absorption) coefficients for arbitrarily shaped nano-particles. The nano-particles can either be free or placed on or in a substrate.

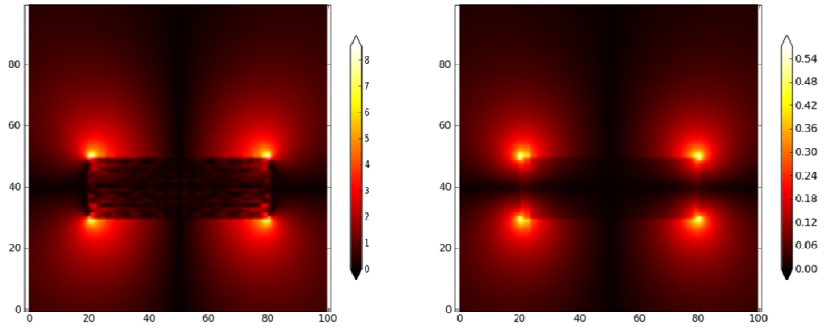

Figure 6. Field interaction comparison for E-field impinging on 50x50x16 nm block of silver (left) and same block with n = 1.5, k=0.01 (right). The block on the left interacts up to 16 times more with the field.

The FDTD software used in this research to solve for metamaterial, photonic crystal and resonator structures is FDTD Solutions by Lumerical, Inc. It provides a solution to Maxwell's equations for discreet time steps at each point of a discreet 3-D mesh made up of Yee cells. Both DDSCAT and FDTD modeling results are compared to experimental results, and to one another.

4. RESULTS

4.1 Mueller-matrix review and canonical experimental results

The Mueller matrix represents the measured system response for conversion of an input Stokes vector to an output Stokes vector. Many practitioners of the DRR measurement technique prefer to present a derived subset of Mueller data such as degree of polarization (DOP) or degree of linear polarization (DOLP) for the measured angular data. We choose to present the data as angularly dependent Mueller matrices with the input-output polarization correlation key shown in Figure 7.[34]

$$S_{Out} = M_{System}\, S_{In}$$

$$\begin{bmatrix} * \\ | \\ / \\ o \end{bmatrix}_{Out} = \begin{bmatrix} *_{Out}\,*_{In} & *_{Out}\,|_{In} & *_{Out}\,/_{In} & *_{Out}\,o_{In} \\ |_{Out}\,*_{In} & |_{Out}\,|_{In} & |_{Out}\,/_{In} & |_{Out}\,o_{In} \\ /_{Out}\,*_{In} & /_{Out}\,|_{In} & /_{Out}\,/_{In} & /_{Out}\,o_{In} \\ o_{Out}\,*_{In} & o_{Out}\,|_{In} & o_{Out}\,/_{In} & o_{Out}\,o_{In} \end{bmatrix}_{System} \begin{bmatrix} * \\ | \\ / \\ o \end{bmatrix}_{In}$$

Figure 7. Linear systems visualization of Mueller matrix interaction. * = Intensity, | = linear vertical polarization, / = +45° polarization, and o = circular polarization.

It is worthwhile to present the two extreme canonical Mueller matrix forms shown in Figure 8, *i.e.* no change in Stokes state and complete loss of Stokes state. It is clear from the operation legend in Figure 7 that the Mueller Identity operation represents an unchanged output Stokes vector. An example of this is taking a transmission DRR measurement without having a sample in place. The depolarization Mueller matrix has all zero values except for M00. All

polarization information is lost. Both of these canonical Mueller matrices are useful for system performance description. Figure 9 shows AFIT DRR measurement results for "Transmissive No Sample" and Spectralon®. Both results are in good agreement with the canonical forms.

$$\begin{bmatrix} * \\ | \\ / \\ o \end{bmatrix}_{Out} = \begin{bmatrix} 1 & 0 & 0 & 0 \\ 0 & 1 & 0 & 0 \\ 0 & 0 & 1 & 0 \\ 0 & 0 & 0 & 1 \end{bmatrix}_{Identity} \begin{bmatrix} * \\ | \\ / \\ o \end{bmatrix}_{In} \qquad \begin{bmatrix} * \\ 0 \\ 0 \\ 0 \end{bmatrix}_{Out} = \begin{bmatrix} 1 & 0 & 0 & 0 \\ 0 & 0 & 0 & 0 \\ 0 & 0 & 0 & 0 \\ 0 & 0 & 0 & 0 \end{bmatrix}_{Depolarizing} \begin{bmatrix} * \\ | \\ / \\ o \end{bmatrix}_{In}$$

Figure 8. (left) Mueller Identity operation – no change in Stokes state. (right) Mueller depolarizer – complete loss of Stokes state.

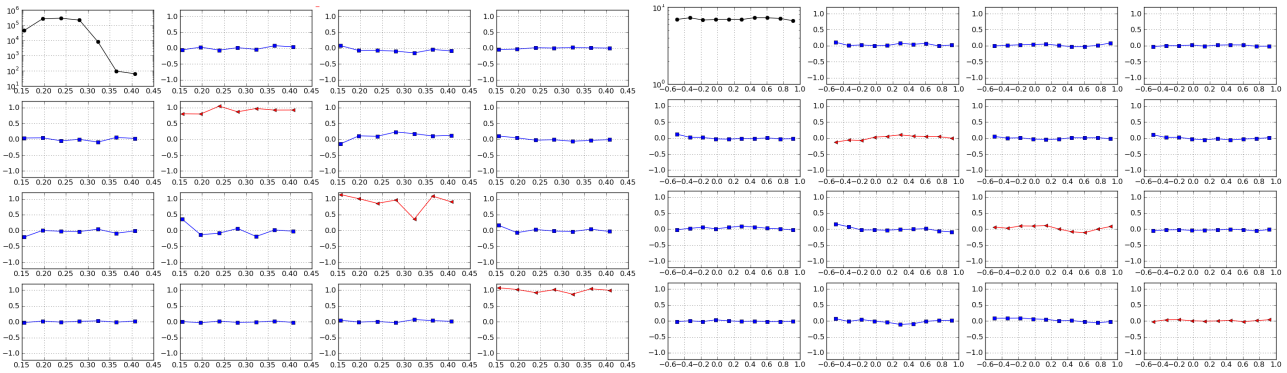

Figure 9. AFIT DRR measurement results for (left) "No Sample" or Mueller Identity operation and (right) Spectralon® diffuse reflector or Mueller depolarizer.

4.2 Mueller distance error metric

The AFIT CASI-DRR instrument was initially assembled in March 2010 and is still going through characterization trials and optical alignment in order to optimize the performance of the instrument. A strong DRR Mueller calculus model has been developed in the Python language to facilitate modeling a measurement and to compare the measurement to the ideal. The residual difference between the measurement and ideal states the sensitivity of the instrument. The residual is given by

$$\varepsilon = \frac{I_{Ideal} - I_{Meas}}{I_{Ideal}} \tag{3}$$

where I is intensity as given in equations (1) and (2). The Mueller distance between Mueller matrices, M_1 and M_2, is a useful tool for measurement comparison to model. The Mueller difference is given by

$$\varepsilon_{1,2} = \sqrt{\frac{\sum_{i,j}^{4,4} (M_{1_{i,j}} - M_{2_{i,j}})^2}{16}} \tag{4}$$

Our typical Mueller distance between current measurement result and the desired identity matrix resulting from measuring the no-sample or "blank" case is 0.064 ± 0.002.[11] For comparison, the calculated Mueller distance for the NIST team led by Germer is 0.0006.[2] We are working to improve our measurement sensitivity and decrease our error metric.

4.3 Silver nanocube modeling results and measurements

An initial application of our technique has been the characterization of a layer of 50-nm silver nanocubes on an ITO-coated glass slide at 544 nm. [35] As shown in Figure 10, the nanocubes are randomly oriented in rotation but are well aligned to the substrate face, and in particular, seem to favor the top-most grain layers. Two SEM micrographs of the nanocubes are shown in Fig. 10 (left and center) with the DDSCAT-derived spectral extinction coefficients of the nanocubes shown on the right. The micrograph on the left shows a sparse concentration of nanocubes with few interacting pairs. The nanocube arrangement shown in the middle has a far higher concentration and will feature interaction between the nanocubes that may significantly modify the scatter pattern. The calculated DDSCAT spectral response clearly shows the additional surface plasmon modes at 417 nm and lower due to the cubic geometry. These are not present in bulk silver.

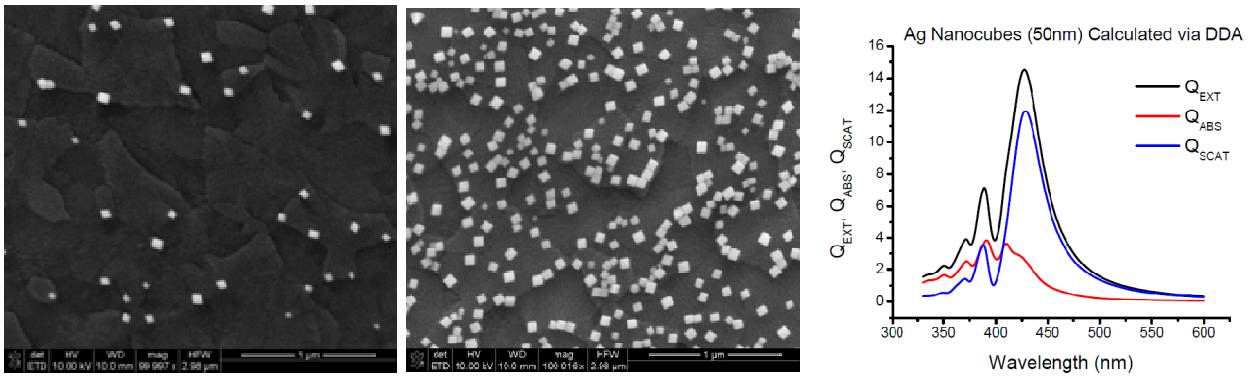

Figure 10. (left and center) Silver nanocubes on glass substrate. (right) DDSCAT calculated scattering coefficients for silver nanocubes.[35]

Figure 11 shows the Lumerical-FDTD-Solutions-calculated wavelength-dependent response as a function of the orientation of a 50-nm silver nanocube rotated about its z-axis. The top and bottom surfaces of the cube are made parallel to the (x,y) plane (defined by the substrate in Figure 11) and the angle of rotation is counterclockwise about the z-axis with respect to the x-axis. The real and imaginary refractive index values of silver were taken from the CRC Handbook of Chemistry and Physics.[1] Because the nanocubes are randomly oriented, it is important to model a single cube at different angles of rotation and average them to find out how a group of randomly orientated, non-interacting cubes interacts with light of different polarization states and angles of incident.

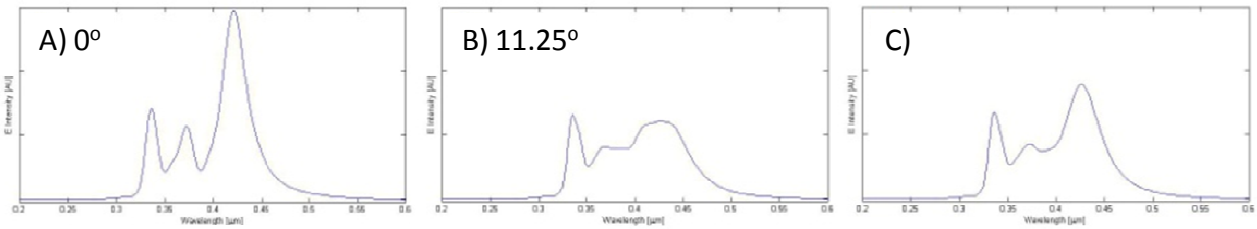

Figure 11. FDTD-calculated values of wavelength-dependent intensity for a 50-nm silver cube illuminated with a plane wave with 45° polarization angle and wavelengths of 300-700 nm injected along the z-axis. The cube was rotated about the z-axis by (A) 0° and (B) 11.25°, and (C) is the non-weighted average for 0°, 11.25°, 22.5°, 33.75° and 45 ° rotations.

Figure 12 (left) shows the measured Mueller-matrix BTDF for the silver nanocubes on an ITO-coated glass slide at 0° angle of incidence. Fig. 12 (right) shows the Mueller-matrix BTDF for the ITO-coated glass slide only. There is a rapid and clear depolarization with increasing angle away from the collinear transmission peak for the silver nanocube sample. This is shown by the decline in BTDF with increasing angle in the diagonal components of Figure 12 (left). This feature is not present in the ITO results with no nanocubes present (Fig. 12 (right)). (We attribute the distinctive up-down pattern between -1 and +1° transmission angle to systematic scatter in the instrument, and are working to decrease this

effect.) Figure 12 shows that a full polarimetric scatter measurement is a useful tool to develop an understanding of the nature of the scatter dependencies for the silver nanocubes. But, it is also clear that probing the silver nanocubes with a spectrally varying input source is necessary in order to probe the desired surface plasmon order.

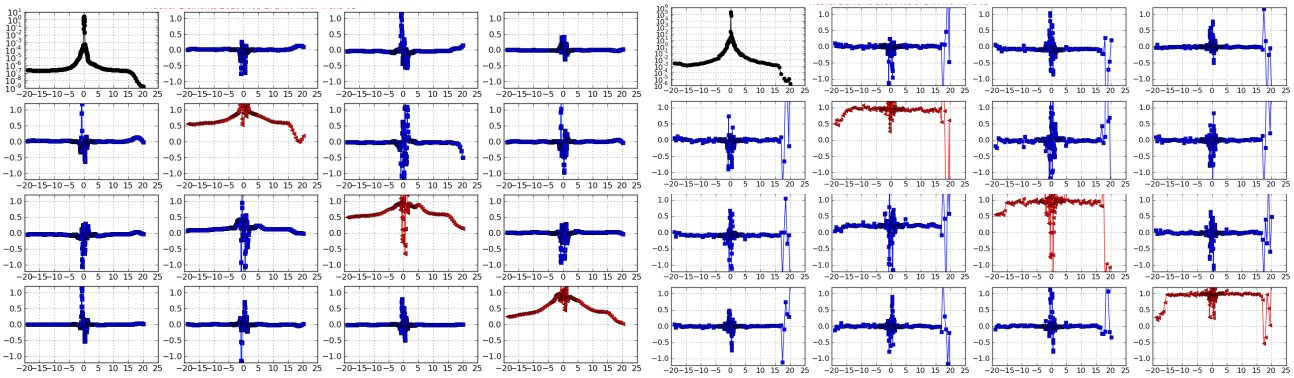

Figure 12. AFIT DRR transmission measurements for (left) nanocubes on ITO-coated glass substrate and (right) an ITO-coated glass substrate.

4.4 Polarimetric Infragold® measurements at 3.39 μm

We completed initial polarimetric Infragold® characterization at 3.39 μm using the AFIT DRR instrument. Infragold® is a diffuse infrared reflectance coating manufactured by Labsphere. It serves an equivalent role in the infrared region as its counterpart, Spectralon ®, does in the visible. *I.e.* it provides a highly Lambertian reflectance standard for comparative measurements. However, there are some pedagogical differences between Infragold® and Spectralon® that non-polarimetric measurements cannot distinguish. Infragold® is a surface scatterer and is dependent on surface micro-roughness for its Lambertian nature. As a consequence, Infragold® retains most polarization state information upon reflection. On the other hand, Spectralon® is a pressed powder and a volume or bulk scatterer. Visible light energy enters the medium and all polarization information is lost during multi-bounce volumetric interaction. The AFIT DRR maintains polarization state information and the diffusely scattering Infragold® is polarimetrically distinguishable from the diffusely scattering Spectralon®. Figure 13 compares AFIT DRR measurements for Infragold at 20° incident angle (right) and the results of a micro-facet reflectance model (left).[36] Infragold® has a Mueller Identity matrix nature whereas Spectralon® has a Mueller depolarizing nature. We are investigating the artifact in the M23 measurement of Infragold® that is not replicated in our model. We believe it is due to preferential-polarization scattering in our instrument.

5. CONCLUSION

We have completed initial development of a full-scatter Dual-Rotating-Retarder ellipsometer suitable for novel metamaterial characterization throughout the MWIR and LWIR. The technique is well suited to capture radiation uniquely scattered by these structures with stated uncertainty limits. The incorporation of predictive computational codes allows us to better analyze measured results and understand the electro-magnetic properties of these materials. We are anxious to apply our resources and instruments to targets of interest to the community.

ACKNOWLEDGMENTS

The authors would like to thank Matthew Niemiec of AFIT for assistance in collecting the data, Nick Herr of AFIT for the nano-patterned polystyrene sample, and Chris Tabor of the Materials and Manufacturing Directorate, Air Force Research Laboratory (AFRL/RX) for the silver nanocube samples. This work was financed by AFRL/RX. The views expressed in this article are those of the authors and do not reflect the official policy or position of the United States Air Force, Department of Defense, or the US Government.

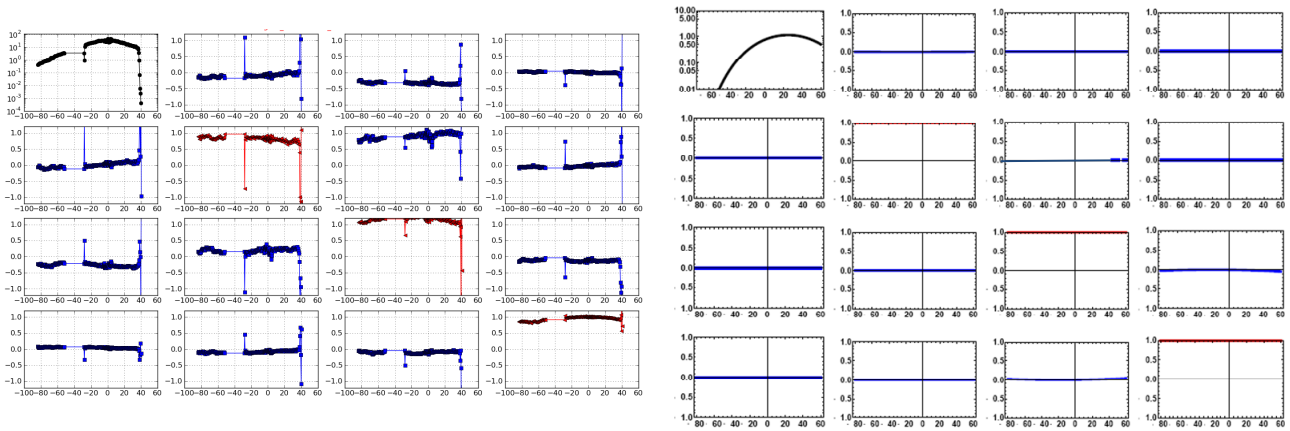

Figure 13. (left) Measured Infragold® Mueller-matrix BRDF for 20° incidence angle at 3.39 μm. (right) Calculated microfacet model Mueller-matrix BRDF for a rough gold surface.

REFERENCES

[1] Ozbay, E. , "Plasmonics: Merging Photonics and Electronics at Nanoscale Dimensions," Science 311(5758), 189-193 (2006).

[2] Germer, T. A. and Asmail, C. C. , "Goniometric optical scatter instrument for out-of-plane ellipsometry measurements," Rev.Sci.Instrum. 70, 3688 (1999).

[3] Germer, T. A. and Fasolka, M. J., "Characterizing surface roughness of thin films by polarized light scattering," Proceedings of SPIE, 264-275 (2003).

[4] Fitzgerald, T. M. and Marciniak, M. A., "Full Optical Scatter Analysis for Novel Photonic and Infrared Metamaterials," *Proceedings of the 13th International Congress and Exposition on Experimental and Applied Mechanics 2010*, Curran Associates, Inc. (2010).

[5] Fitzgerald, T. M. and Marciniak, M. A., "Full Scatter Characterization of Novel Photonic and Infrared Metamaterials," *"Electromagnetic meta-materials," Proceedings of the International Symposium, "Electromagnetic meta-materials" of the Forum on New Materials, part of CIMTEC 2010 - 12th International Ceramics Congress and 5th Forum on New Materials* (2010).

[6] Smith, D. R., Schultz, S., Markoš, P. and Soukoulis, C. M. , "Determination of effective permittivity and permeability of metamaterials from reflection and transmission coefficients," Physical Review B 65(19), 195104 (2002).

[7] Azzam, R. M. A. and Bashara, N. M., [Ellipsometry and Polarized Light], North-Holland (1977).

[8] Goldstein, D. H. and Chipman, R. A. , "Error analysis of a Mueller matrix polarimeter," Journal of the Optical Society of America A 7(4), 693-700 (1990).

[9] Smith, M. H. , "Optimization of a dual-rotating-retarder Mueller matrix polarimeter," Appl.Opt. 41, 2488-2493 (2002).

[10] Technical Staff, D. S. (2010).

[11] Chipman, R. A. , "Handbook of Optics, vol. II, ch. 22," Optical Society of America, (2000).

[12] Compain, E., Poirier, S. and Drevillon, B. , "General and self-consistent method for the calibration of polarization modulators, polarimeters, and Mueller-matrix ellipsometers," Appl.Opt. 38, 3490-3502 (1999).

[13] Chenault, D. B. and Chipman, R. A. , "Measurements of linear diattenuation and linear retardance spectra with a rotating sample spectropolarimeter," Appl.Opt. 32(19), 3513-3519 (1993).

[14] Draine, B. T., "The discrete-dipole approximation and its application to interstellar graphite grains," Astrophys.J. 333 (Part 1), (1988).

[15] Draine, B. T. and Flatau, P. J. , "Discrete-dipole approximation for scattering calculations," JOURNAL-OPTICAL SOCIETY OF AMERICA A 11, 1491-1491 (1994).

[16] Draine, B. T. and Flatau, P., "User Guide for the Discrete Dipole Approximation Code DDSCAT 7.0," eprint arXiv: 0809.0337 (2008).

[17] Noguez, C. , "Surface plasmons on metal nanoparticles: the influence of shape and physical environment," J.Phys.Chem.C 111, 3806-3819 (2007).

[18] Noguez, C., Roman-Velazquez, C. E., Esquivel-Sirvent, R. and Villarreal, C. , "High-multipolar effects on the Casimir force: The non-retarded limit," Europhys.Lett. 67(2), 191-197 (2004).
[19] Noguez, C., Sosa, I. O., Barrera, R. G. and DF, M., "Light Scattering by Isolated Nanoparticles With Arbitrary Shapes," MATERIALS RESEARCH SOCIETY SYMPOSIUM PROCEEDINGS, 275-280 (2001).
[20] Sosa, I. O., Noguez, C. and Barrera, R. G. , "Optical Properties of Metal Nanoparticles with Arbitrary Shapes," J Phys Chem B 107(26), 6269-6275 (2003).
[21] Cho, D., Wang, F., Zhang, X. and Shen, Y. R., "Contribution of electric quadrupole resonance in optical metamaterials," American Physical Society, 2008 APS March Meeting, March 10-14, 2008, abstract# D35. 012 (2008).
[22] Cai, W., Chettiar, U. K., Kildishev, A. V. and Shalaev, V. M., "Optical Cloaking with Non-Magnetic Metamaterials," Arxiv preprint physics/0611242 (2006).
[23] Cai, W., Chettiar, U. K., Kildishev, A. V. and Shalaev, V. M. , "Optical cloaking with metamaterials," Nature Photonics 1, 224–226 (2007).
[24] Chettiar, U. K., Kildishev, A. V., Yuan, H. K., Cai, W., Xiao, S., Drachev, V. P. and Shalaev, V. M., "Dual-Band Negative Index Metamaterial: Double-Negative at 813 nm and Single-Negative at 772 nm," (2008).
[25] Hicks, E. M., Lyandres, O., Hall, W. P., Zou, S., Glucksberg, M. R. and Van Duyne, R. P. , "Plasmonic Properties of Anchored Nanoparticles Fabricated by Reactive Ion Etching and Nanosphere Lithography," Journal of physical chemistry.C 111(11), 4116-4124 (2007).
[26] Penttilä, A., Zubko, E., Lumme, K., Muinonen, K., Yurkin, M. A., Draine, B., Rahola, J., Hoekstra, A. G. and Shkuratov, Y. , "Comparison between discrete dipole implementations and exact techniques," Journal of Quantitative Spectroscopy and Radiative Transfer 106(1-3), 417-436 (2007).
[27] Diana, F. S., David, A., Meinel, I., Sharma, R., Weisbuch, C., Nakamura, S. and Petroff, P. M. , "Photonic crystal-assisted light extraction from a colloidal quantum Dot/GaN hybrid structure," Nano Letters 6(6), 1116-1120 (2006).
[28] Sherry, L. J., Jin, R., Mirkin, C. A., Schatz, G. C. and Van Duyne, R. P. , "Localized surface plasmon resonance spectroscopy of single silver triangular nanoprisms," Nano Lett 6(9), 2061 (2006).
[29] Sherry, L. J., Chang, S. H., Schatz, G. C., Van Duyne, R. P., Wiley, B. J. and Xia, Y. , "Localized surface plasmon resonance spectroscopy of single silver nanocubes," Nano Lett 5(10), 2034–2038 (2005).
[30] Byun, K., Kim, S. and Kim, D. , "Design study of highly sensitive nanowire-enhanced surface plasmon resonance biosensors using rigorous coupled wave analysis," Optics Express 13(10), 3737-3742 (2005).
[31] Lu, J., Petre, C., Yablonovitch, E. and Conway, J. , "Numerical optimization of a grating coupler for the efficient excitation of surface plasmons at an Ag-SiO_2 interface," Journal of the Optical Society of America B 24(9), 2268-2272 (2007).
[32] Moharam, M. G. and Gaylord, T. K., [Rigorous Coupled-Wave Analysis of Planar-Grating Diffraction], OSA (1980).
[33] Spiegel, J., de la Torre, J., Darques, M., Piraux, L. and Huynen, I. , "Permittivity Model for Ferromagnetic Nanowired Substrates," IEEE Microwave and Wireless Components Letters 17(7), 492 (2007).
[34] Kokhanovsky, A. A., [Polarization Optics of Random Media], Springer Verlag (2003).
[35] Mahmoud, M. A., Tabor, C. E. and El-Sayed, M. A. , "Surface-Enhanced Raman Scattering Enhancement by Aggregated Silver Nanocube Monolayers Assembled by the Langmuir-Blodgett Technique at Different Surface Pressures," J.Phys.Chem.C 113, 5493 (2009).
[36] Priest, R. G. and Germer, T. A. , "Polarimetric BRDF in the microfacet model: Theory and measurements," TR, Naval Research Laboratory, Washington DC (2000).